scientific reports

Check for updates

OPEN

Chloride electrode composed of ubiquitous elements for high-energy-density all-solid-state sodium-ion batteries

Naoto Tanibata✉, Naoki Nonaka, Keisuke Makino, Hayami Takeda & Masanobu Nakayama

Inexpensive and safe energy-storage batteries with high energy densities are in high demand (e.g., for electric vehicles and grid-level renewable energy storage). This study focused on using $NaFeCl_4$, comprising ubiquitous elements, as an electrode material for all-solid-state sodium-ion batteries. Monoclinic $NaFeCl_4$, expected to be the most resource-attractive Fe redox material, is also thermodynamically stable. The $Fe^{2+/3+}$ redox reaction of the monoclinic $NaFeCl_4$ electrode has a higher potential (3.45 V vs. Na/Na^+) than conventional oxide electrodes (e.g., Fe_2O_3 with 1.5 V vs. Na/Na^+) because of the noble properties of chlorine. Additionally, $NaFeCl_4$ exhibits unusually high deformability (99% of the relative density of the pellet) upon uniaxial pressing (382 MPa) at 298 K. $NaFeCl_4$ operates at 333 K in an electrode system containing no electrolyte, thereby realizing next-generation all-solid-state batteries with high safety. A high energy density per positive electrode of 281 Wh kg^{-1} was achieved using only a simple powder press.

The demand for energy-storage batteries to realize a sustainable society is increasing annually[1]. Lithium-ion batteries are used in various portable devices because of their high working potentials (> 3 V)[2]. However, the low abundance of lithium and redox-center transition metals (such as Co and Ni)[3,4] and their environmental impact, such as the soil contamination associated with their extraction, have become problematic[5]. Alternative solutions that have been proposed for these problems include the use of sodium-ion batteries, which are composed of ubiquitous elements, including sodium as the carrier ion, which has chemical properties similar to those of lithium, such as a high ionization tendency and stable monovalent ions[6,7]. In addition, commercially available lithium-ion batteries currently use flammable organic electrolytes, and their safety is a concern as their application in electric vehicles and large storage batteries continues to advance. In view of these concerns, all-solid-state batteries (ASSBs), which have inorganic solid electrolytes, are expected to be used as next-generation batteries because of their highly improved safety[8–10]. Furthermore, because ASSBs do not contain liquid electrolytes, new electrode materials like elemental sulfur and chloride, which would otherwise leach into the liquid electrolyte, can be used, thereby creating the possibility of increasing the energy density beyond those of conventional batteries[11,12].

Chlorides are being extensively studied as solid electrolytes for ASSBs[13,14]. Compared to compounds with divalent anions, such as oxides and sulfides, which have received widespread attention, anionic compounds with a univalent anion, such as chlorides, undergo limited Coulombic interactions with carrier ions, which have high diffusivity[15]. Unlike oxides, chloride ions tend to exhibit high polarizability and deformability, similar to that of sulfides[16–18]. High deformability enables the use of a sinterless compaction process, which is advantageous for the fabrication of ASSBs[19]. The disadvantage of the use of sintering for densification is that it is inapplicable to certain materials owing to side reactions[20] and the evaporation of elements[21,22].

An additional benefit of chloride is that it is a promising electrolyte, particularly in cathodes, owing to its higher oxidation resistance (~ 4.0 V vs. Li/Li^+) than those of sulfide (~ 2.5 V vs. Li/Li^+) and oxide (~ 3.5 V vs. Li/Li^+), which has its origins in the noble properties of chlorine[23,24]. This high resistance to oxidation is a feature of the high working potential required for high energy density when used in electrode materials. As mentioned previously, the high polarity of chloride electrolytes often causes dissolution of the constituent elements in the electrolyte solution when they are used as liquid electrolytes. This severely affects the cycle life of the battery because it lowers the number of reversible charge–discharge cycles. However, the dissolution reaction of chloride

Department of Advanced Ceramics, Nagoya Institute of Technology, Gokiso, Showa, Nagoya, Aichi 466-8555, Japan. ✉email: tanibata.naoto@nitech.ac.jp

electrodes is suppressed when they are used in combination with solid electrolytes; thus, chloride electrodes are potentially suitable for use as high-voltage cathode materials for rechargeable ASSBs.

In this study, we focused on $NaFeCl_4$ as an electrode material for ASSBs, because $NaFeCl_4$ contains sodium chloride and the ubiquitous element Fe as the transition metal in the redox center. $NaFeCl_4$ is registered on the ISCD (#16994)[25] and has an orthorhombic crystal structure (*S.G.*: $P2_12_12_1$), with Fe in the center of the tetrahedron formed by the chloride ions. In electrode materials based on the $Fe^{2+/3+}$ redox reaction, $Na_2Fe_2(SO_4)_3$[26] exhibited a higher potential (3.8 V vs. Na/Na^+) than conventional oxide electrodes (Fe_2O_3[27], 1.5 V vs. Na/Na^+) because of the noble properties of the SO_4^{2-} unit (which has an inductive effect). The same effect that was induced by the SO_4^{2-} ion was expected for the lighter Cl^- ion (molar mass per charge Cl^-: 34.5 g mol^{-1}, (SO_4^{2-})/2:48 g mol^{-1}), and the charge–discharge properties of the $Fe^{2+/3+}$ redox pair were evaluated at the $NaFeCl_4$ electrode. The theoretical capacity of this material is 121 mAh g^{-1} at one Na per $NaFeCl_4$ formula unit. We also assembled an ASSB using an electrode without electrolyte added to the electrode composite (hereafter referred to as an "electrolyte-free electrode"). Conventional oxide electrodes exhibit low deformability and can be fabricated by adding soft sulfide electrolytes or other materials. However, the addition of electrolytes has the effect of decreasing the theoretical energy density per electrode composite, in which case the reaction distribution becomes more complicated. For chloride electrodes, the active material in the electrode may have high deformability. Therefore, in ASSBs, the electrode composites that do not contain solid electrolyte powders may surpass conventional battery systems in terms of their energy density.

Results and discussion

Structure and deformability

The X-ray diffraction (XRD) pattern of the synthesized $NaFeCl_4$ sample (Fig. 1a) indicates a single phase consisting of monoclinic $NaFeCl_4$. The peaks of the raw material are no longer visible. The relative density of the uniaxially compressed pellet was calculated from the apparent density of the compact and crystal lattice density of the monoclinic $NaFeCl_4$ (2.31 g cm^{-3}). The value of 99.1% for $NaFeCl_4$ (at 382 MPa) is higher than those for Li_2FeCl_4 (92% at 382 MPa)[28] and Li_3TiCl_6 (86.1% at 350 MPa)[29], which have recently been reported as highly deformable electrodes. The cross-sectional scanning electron microscopy (SEM) image of the $NaFeCl_4$ powder compact (Fig. 1b) indicates that the grains were crushed by compaction, resulting in a dense structure with ill-defined grain boundaries. These results indicate that the $NaFeCl_4$ powder has high deformability.

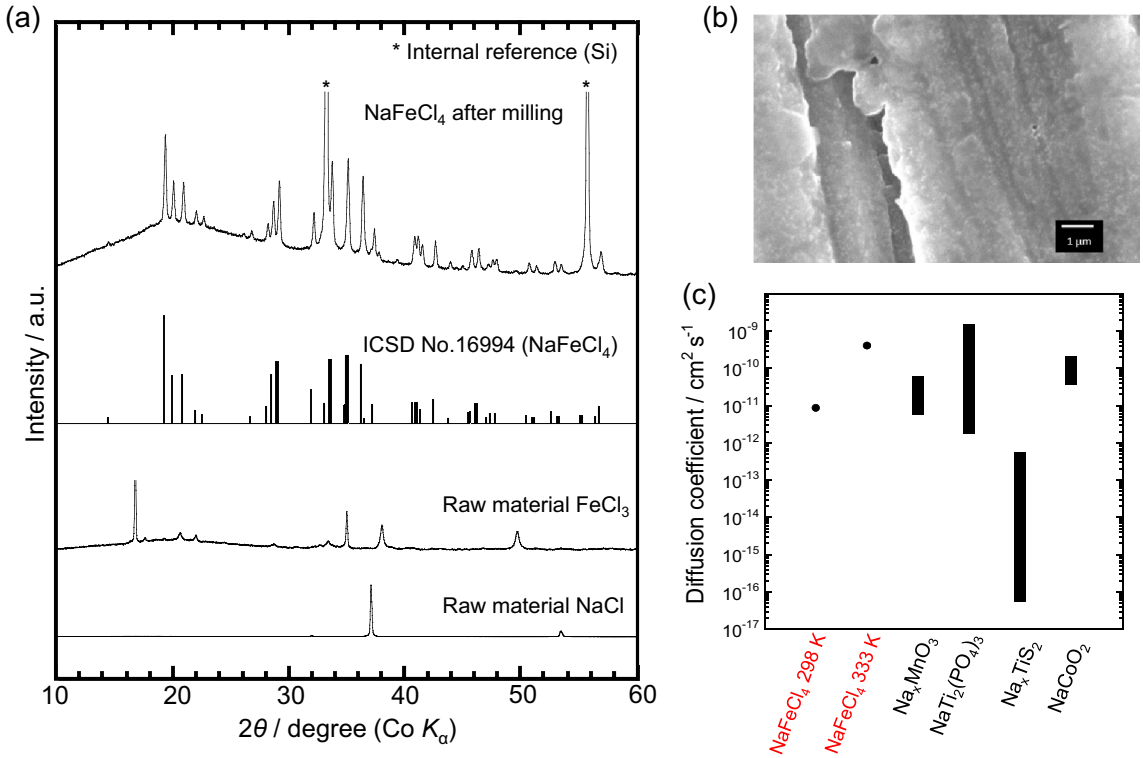

Figure 1. Characterization of synthesized $NaFeCl_4$. (**a**) XRD patterns of $NaFeCl_4$ after milling and the raw material and the simulated pattern of orthorhombic $NaFeCl_4$ from the ICSD database (#16994). (**b**) Cross-sectional SEM image of the pellet uniaxially compressed. (**c**) Conductivity diffusion coefficient of $NaFeCl_4$ obtained from AC impedance measurements at 298 and 333 K and the chemical diffusion coefficients of typical oxide (Na_xMnO_3[30],$NaTi_2(PO_4)_3$[31],and $NaCoO_2$[32]) and sulfide (Na_xTiS_2[33]) cathode materials at room temperature.

Electrochemical performance

An ASSB with a solid electrolyte was fabricated to evaluate this strongly ionic electrode-active material without it leaching into the electrolyte. In addition, taking advantage of this deformability, electrolyte-free electrodes were fabricated for application in ASSBs, and their charge–discharge characteristics were evaluated. Based on the conductivity diffusion coefficient (Fig. 1c) obtained from the impedance plot (Supplementary Fig. 1), the battery operating temperature was set at 333 K to ensure that the diffusion coefficient is higher than those of conventional electrode materials. The solid electrolyte ($Na_3PS_4|Na_{2.25}Y_{0.25}Zr_{0.75}Cl_6$) consists of two layers, one on the anode ($Na_{10}Sn_4$) side and the other on the cathode ($NaFeCl_4$) side, to suppress the reactions between the electrodes and electrolytes (cell configuration: $Na_{10}Sn_4$ + acetylene black (AB)$|Na_3PS_4|Na_{2.25}Y_{0.25}Zr_{0.75}Cl_6|NaFeCl_4$ + KB) based on an examination of reactions like the oxidation of Na_3PS_4, as shown in Supporting Section 1 (Supplementary Figs. S2 and S3). The resulting reversible capacity was 90.8 mAh $(g\text{-}NaFeCl_4)^{-1}$ (81.7 mAh $(g\text{-positive electrode})^{-1}$), and the average working potential was ~ 3.45 V (vs. Na/Na^+), as is evident from the constant-current charge–discharge curves (Fig. 2a) and the dQ/dV curves (Figure S4).

The results of the impedance measurements (Fig. 2b) indicate only a small semicircular resistance and no significant increase in the first charge–discharge process or after the cycle test. The battery also exhibits relatively stable cycling characteristics over 10 cycles (Fig. 2c). Based on the reversible capacity of this discharge capacity (~ 90 mAh g^{-1}), the gravimetric energy density per positive electrode was calculated to be 281 Wh kg^{-1} at the reference potential of Na (~ 3.45 V). In Table 1, this value is compared with previously reported energy densities of bulk ASSBs with high-potential operation (> 3 V). This shows that the ASSB fabricated in this study via a simple process using only pressed powders, which does not require any coating or sintering process on the

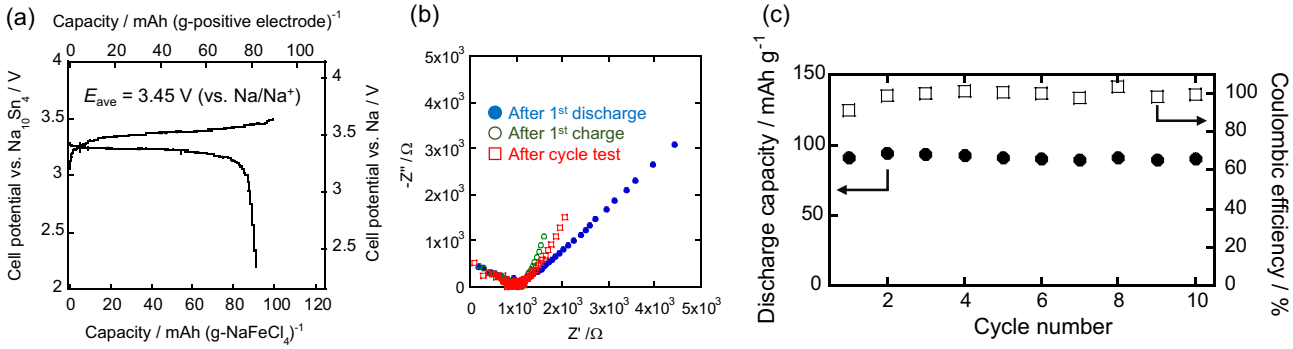

Figure 2. Characteristics of the ASSB ($Na_{10}Sn_4$ + AB$|Na_3PS_4|Na_{2.25}Y_{0.25}Zr_{0.75}Cl_6|NaFeCl_4$ + KB) using a $NaFeCl_4$ electrode without electrolyte ($NaFeCl_4$:KB = 90:10 wt%) and with the bilayer electrolyte ($Na_3PS_4|Na_{2.25}Y_{0.25}Zr_{0.75}Cl_6$). (**a**) Constant-current charge–discharge curves. (**b**) Impedance plots before and after charging and discharging. (**c**) Cycle characteristics of discharge capacity (circle) and Coulombic efficiency (square).

Report	E_m (Wh kg^{-1})	Cathode active material (CAM)	Type of solid electrolyte	Solid electrolyte (SE)	Weight ratio of cathode (CAM:SE:others)	Preparation	Operating temperature (K)
This experimental	281	$NaFeCl_4$	Inorganic	Na_3PS_4 and $Na_{2.25}Y_{0.25}Zr_{0.75}Cl_6$	90:0:10	Power compress	333
Zhang et al.[34]	278	$Na_3V_2P_3O_{12}$		La-substituted $Na_3Zr_2Si_2PO_{12}$	65:15:20	Sintering	353
Duchêne et al.[35]	185	$NaCrO_2$		$Na_4(B_{12}H_{12})(B_{10}H_{10})$	70:20:10	Power compress	303
Yamauchi et al.[36]	173	Na_2O-Fe_2O_3-P_2O_5 glass		β"—Al_2O_3	72:25:3	Sintering	303
Hayashi et al.[37]	91.6	$NaCrO_2$		Na_3PS_4	36:55:9	Power compress	303
Niu et al.[38]	169	$C_2H_4(CN)_2$-$NaClO_4$ coated $Na_{0.67}Ni_{0.33}Mn_{0.67}O_2$	Polymer & Inorganic	Polyethylene Oxide-$Na_3Zr_2Si_2PO_{12}$-$NaClO_4$	70:0:30	Power compress	328
Yao et al.[39]	288	$Na_3V_2P_3O_{12}$	Polymer	Polyethylene glycol dimethacrylate -NaFSI	70:20:10	Power compress	333
Yu et al.[40]	237	$Na_2MnFe(CN)_6$		Polyethylene Oxide-$NaClO_4$-$Na_3Zr_2Si_2PO_{12}$	55:18:27	Power compress	333
Zhao et al.[41]	220	$Na_3V_2P_3O_{12}$		Polyethylene Oxide-NaFSI	60:10:30	Power compress	353

Table 1. Comparison of the energy density per positive electrode weight, E_m[a], of the ASSB in this study with that of other bulk ASSB with a high-potential cathode (> 3 V). [a]E_m is the energy density per positive electrode weight assuming a Na metal anode. If not stated otherwise, it was calculated from the initial discharge curve. Other information, such as the materials used, their mixing ratios, fabrication conditions, and working temperatures, is also shown.

surface of the cathode active material, has higher energy density than other reported bulk ASSBs using inorganic and/or polymer electrolytes.

The redox mechanism of the $NaFeCl_4$ electrode was investigated by X-ray photoelectron spectroscopy (XPS) before and after the charge–discharge process. The Fe 2p XPS profile (Fig. 3) consists of two sets of doublet peaks (Fe $2p_{3/2}$ and Fe $2p_{1/2}$) and their satellite peaks. Deconvolution of each spectrum using the pseudo-Voigt function revealed that the Fe $2p_{2/3}$ peak is located near 711.0 eV before and after charge, whereas a high-intensity peak appears near 710.5 eV, and the intensity of the peak at 711.0 eV is lower after discharge. The Fe $2p_{2/3}$ peaks of $FeCl_2$ and $FeCl_3$ in the reference sample appear at 710.6 eV and 711.3 eV, respectively[42,43], with the low- and high-energy peaks attributable to Fe^{2+} and Fe^{3+}, respectively. The peak ratio after discharge was approximately 3:1, which is consistent with the fact that the discharge capacity was approximately 75% of the theoretical capacity (121.5 mAh g^{-1}). This indicates that the charge–discharge process proceeded via the redox reaction of $Fe^{2+/3+}$ in $NaFeCl_4$. As mentioned previously, the redox reaction of $Fe^{2+/3+}$ has been reported to have a low potential of approximately 1.5 V in conventional oxides (Fe_2O_3). In this material, the inductive effect of chlorine may be responsible for the higher potential (3.45 V vs. Na/Na^+), which would be responsible for the high energy density listed in Table 1. The XPS profile after charging revealed a reversible return to the original Fe^{3+} state before the charge–discharge process. The XRD patterns before and after charging (Supplementary Fig. S4) also show a reversion to monoclinic $NaFeCl_4$, indicating the occurrence of a reversible charge–discharge reaction involving a $Fe^{2+/3+}$ redox reaction. The synthesis of Na_2FeCl_4, which can be charge-started, has not yet been reported; therefore, it is expected to be evaluated in future studies.

In summary, the $NaFeCl_4$ electrode, composed of ubiquitous elements, was evaluated for application in a low-cost storage battery with high energy density and safety. An ASSB was operated at 333 K with an electrolyte-free electrode owing to the high deformability derived from chloride ions (relative density = 99% of the pellet uniaxially compressed at 298 K). In addition, owing to the inductive effect of chloride, high-potential operation (3.45 V vs. Na/Na^+) was demonstrated with the most attractive Fe redox reaction ($Fe^{2+/3+}$) in terms of the elemental strategy. Consequently, an outstanding energy density (281 Wh (kg-positive electrode)$^{-1}$) was achieved for conventional bulk all-solid-state sodium-ion batteries without sintering or electrode coating treatment. This study demonstrates the potential of NaCl-based materials as high-energy-density electrode materials, which have previously been difficult to evaluate because of their elution into the electrolyte.

Methods

Preparation and evaluation of all-solid-state cells using $NaFeCl_4$ electrodes

$NaFeCl_4$ was synthesized from NaCl (Wako Pure Chemical Industries, Ltd., 99.5%) and $FeCl_3$ (Sigma-Aldrich Japan LLC, 99.9%) powders by a mechanochemical method[28]. A stoichiometric mixture was placed in a 45 mL

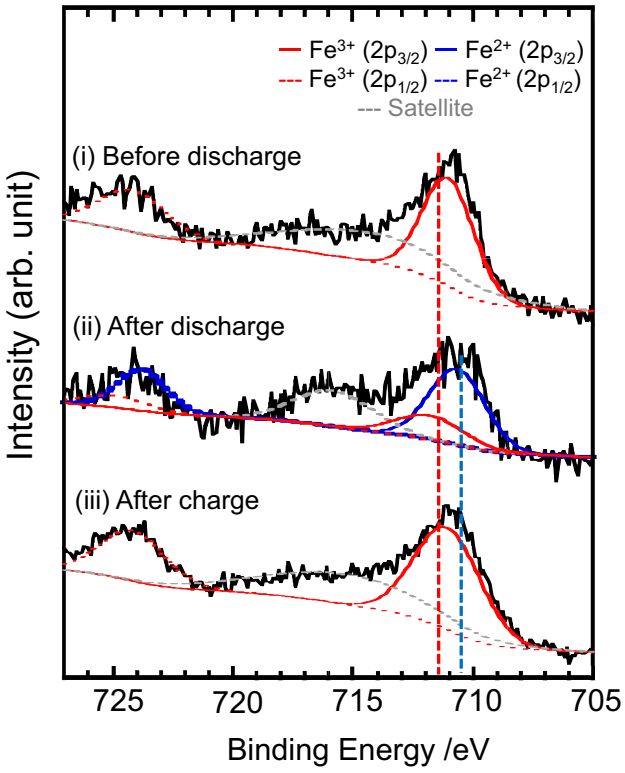

Figure 3. Fe 2p XPS results of the $NaFeCl_4$ electrode before and after the charge–discharge process. The spectra were fitted with $2p_{3/2}$ and $2p_{1/2}$ of $Fe^{2+/3+}$ and satellite peaks.

stainless steel pot with 74 ZrO_2 balls (diameter = 5 mm) and milled using a planetary ball mill apparatus (Fritsch Japan Co., Ltd., P-7 classic-line, Japan) at a rotation speed of 300 rpm for 5 h. The as-produced yellow sample was probed by XRD (MiniFlex 600, Rigaku, Japan, Co*K*α line). The conductivity diffusion coefficient was measured at 298 and 333 K using the AC impedance method (VSP Potentiostat, BioLogic, France) with an AC voltage of 300 mV and a measurement frequency range of 10^2–10^6 Hz. Pellets (diameter = 10 mm, thickness = ~0.50 mm) were prepared by sandwiching the powder between stainless steel plates and compressing under 382 MPa at 298 K. The pellets contain 10 wt% of Ketjen black (KB) as a conductivity aid. The cross-section of a pellet was polished with a #2000 file, and cross-sectional images were acquired using SEM (JSM-6360LV, JEOL, Japan) at a voltage of 10 kV. All the procedures were performed under dry Ar gas.

Electrolyte-free electrodes were prepared with $NaFeCl_4$, and the charge–discharge characteristics of the all-solid-state sodium-ion batteries were evaluated. The $NaFeCl_4$ electrode was mixed with KB (mixing ratio of $NaFeCl_4$:KB = 90:10 wt%) as a conductive aid via ball milling at 300 rpm for 1 h. The solid electrolyte was the sulfide Na_3PS_4[44] and/or chloride $Na_{2.25}Y_{0.25}Zr_{0.75}Cl_6$[45], and the negative electrode (counter electrode) was $Na_{10}Sn_4$-AB (AB: acetylene black; mixing ratio of $Na_{10}Sn_4$:AB = 90:10 wt%)[46]. For cell fabrication, approximately 60 mg of the electrolyte was first placed in a polycarbonate pressure vessel with a cylindrical inner diameter of 10 mm, sandwiched between two pieces of stainless steel, and pressurized to 96 MPa. Subsequently, the cathode material was placed on one side and pressed at 96 MPa, whereas the anode material was placed on the other side and pressed at 382 MPa. The cells were then screwed in from the top and bottom and restrained. When two layers of the electrolyte were used, approximately 30 mg of the Na_3PS_4 electrolyte was used on the anode side and approximately 30 mg of the $Na_{2.25}Y_{0.25}Zr_{0.75}Cl_6$ electrolyte on the cathode side. Charging and discharging were evaluated using a potentiostat/galvanostat (VSP Potentiostat, BioLogic, France) at a temperature of 333 K, current density of 6.4 μA cm^{-2}, and starting from the discharging process (Na storage). AC impedance measurements were performed in the frequency range of 1 – 10^6 Hz after charging and discharging. The charge–discharge mechanism of $NaFeCl_4$ was investigated by conducting Fe 2p XPS measurements on the electrode before and after charging and discharging using a Cr K_α radiation source (PHI Quantes, ULVAC-PHI, Inc., USA) without surface etching treatment, which would be a concern in terms of alteration.

Data availability

All relevant data are available from the corresponding author on reasonable request.

Received: 4 September 2023; Accepted: 29 January 2024
Published online: 01 February 2024

References

1. Larcher, D. & Tarascon, J.-M. Towards greener and more sustainable batteries for electrical energy storage. *Nat. Chem.* **7**, 19–29 (2015).
2. Manthiram, A. An outlook on lithium ion battery technology. *ACS Cent. Sci.* **3**, 1063–1069 (2017).
3. Carmichael, R. S. *Revival: Practical Handbook of Physical Properties of Rocks and Minerals* (CRC Press, 1989).
4. Abraham, K. M. How comparable are sodium-ion batteries to lithium-ion counterparts?. *ACS Energy Lett.* **5**, 3544–3547 (2020).
5. Schmidt, T., Buchert, M. & Schebek, L. Investigation of the primary production routes of nickel and cobalt products used for Li-ion batteries. *Resour. Conserv. Recycl.* **112**, 107–122 (2016).
6. Yabuuchi, N., Kubota, K., Dahbi, M. & Komaba, S. Research development on sodium-ion batteries. *Chem. Rev.* **114**, 11636–11682 (2014).
7. Tanibata, N. *et al.* Nanotube-structured $Na_2V_3O_7$ as a cathode material for sodium-ion batteries with high-rate and stable cycle performances. *Sci. Rep.* **8**, 17199 (2018).
8. Kundu, D., Talaie, E., Duffort, V. & Nazar, L. F. The emerging chemistry of sodium ion batteries for electrochemical energy storage. *Angewandte Chemie Int. Ed.* **54**, 3431–3448 (2015).
9. Harada, M. *et al.* Bayesian-optimization-guided experimental search of NASICON-type solid electrolytes for all-solid-state Li-ion batteries. *J. Mater. Chem. A Mater.* **8**, 15103–15109 (2020).
10. Sun, Y.-K. Promising all-solid-state batteries for future electric vehicles. *ACS Energy Lett.* **5**, 3221–3223 (2020).
11. Wang, K., Gu, Z., Xi, Z., Hu, L. & Ma, C. Li_3TiCl_6 as ionic conductive and compressible positive electrode active material for all-solid-state lithium-based batteries. *Nat. Commun.* **14**, 1396 (2023).
12. Tanibata, N., Deguchi, M., Hayashi, A. & Tatsumisago, M. All-solid-state Na/S batteries with a Na_3PS_4 electrolyte operating at room temperature. *Chem. Mater.* **29**, 5232–5238 (2017).
13. Tanibata, N. *et al.* Metastable chloride solid electrolyte with high formability for rechargeable all-solid-state lithium metal batteries. *ACS Mater. Lett.* **2**, 880–886 (2020).
14. Wu, E. A. *et al.* A stable cathode-solid electrolyte composite for high-voltage, long-cycle-life solid-state sodium-ion batteries. *Nat. Commun.* **12**, 1256 (2021).
15. Wang, S. *et al.* Lithium chlorides and bromides as promising solid-state chemistries for fast ion conductors with good electrochemical stability. *Angewandte Chemie Int. Ed.* **58**, 8039–8043 (2019).
16. Ashcroft, N. W. & Mermin, N. D. *Solid State Physics* (Holt, Rinehart and Winston, 1976).
17. Pauling, L. The nature of the chemical bond. IV. The energy of single bonds and the relative electronegativity of atoms. *J. Am. Chem. Soc.* **54**, 3570–3582 (1932).
18. Aizu, S. *et al.* Screening chloride Li-ion conductors using high-throughput force-field molecular dynamics. *J. Am. Ceram. Soc.* **106**, 3035–3044 (2023).
19. Kato, Y. *et al.* High-power all-solid-state batteries using sulfide superionic conductors. *Nat. Energy* **1**, 1–7 (2016).
20. Kim, K. H. *et al.* Characterization of the interface between $LiCoO_2$ and $Li_7La_3Zr_2O_{12}$ in an all-solid-state rechargeable lithium battery. *J. Power Sources* **196**, 764–767 (2011).
21. Chen, K., Shen, Y., Zhang, Y., Lin, Y. & Nan, C. W. High capacity and cyclic performance in a three-dimensional composite electrode filled with inorganic solid electrolyte. *J. Power Sources* **249**, 306–310 (2014).
22. Takeda, H. *et al.* Process optimisation for NASICON-type solid electrolyte synthesis using a combination of experiments and bayesian optimisation. *Mater. Adv.* **3**, 8141–8148 (2022).
23. Qie, Y. *et al.* Yttrium-sodium halides as promising solid-state electrolytes with high ionic conductivity and stability for Na-ion batteries. *J. Phys. Chem. Lett.* **11**, 3376–3383 (2020).

24. Allen, L. C. Electronegativity is the average one-electron energy of the valence-shell electrons in ground-state free atoms. *J. Am. Chem. Soc.* **111**, 9003–9014 (2002).
25. Richards, R. R. & Gregory, N. W. The crystal structure of sodium tetrachloroferrate(III). *J. Phys. Chem.* **69**, 239–244 (1965).
26. Barpanda, P., Oyama, G., Nishimura, S. I., Chung, S. C. & Yamada, A. A 3.8-V earth-abundant sodium battery electrode. *Nat. Commun.* **5**, 4358 (2014).
27. Chen, M. *et al.* A movable Fe_2O_3 core in connected hierarchical pores for ultrafast intercalation/deintercalation in sodium-ion batteries. *ACS Appl. Energy Mater.* **4**, 5888–5896 (2021).
28. Tanibata, N. *et al.* High formability and fast lithium diffusivity in metastable spinel chloride for rechargeable all-solid-state lithium-ion batteries. *Adv. Energy Sustain. Res.* **1**, 2000025 (2020).
29. Wang, K., Gu, Z., Xi, Z., Hu, L. & Ma, C. Li_3TiCl_6 as ionic conductive and compressible positive electrode active material for all-solid-state lithium-based batteries. *Nat. Commun.* **14**, 1–10 (2023).
30. Xu, Y. *et al.* Enhancement of sodium ion battery performance enabled by oxygen vacancies. *Angewandte Chemie Int. Ed.* **54**, 8768–8771 (2015).
31. Yu, P., Li, C. & Guo, X. Sodium storage and pseudocapacitive charge in textured $Li_4Ti_5O_{12}$ thin films. *J. Phys. Chem. C* **118**, 10616–10624 (2014).
32. Shibata, T., Fukuzumi, Y., Kobayashi, W. & Moritomo, Y. Fast discharge process of layered cobalt oxides due to high Na+ diffusion. *Sci. Rep.* **5**, 9006 (2015).
33. Sayed, F. N. *et al.* Li and Na-ion diffusion and intercalation characteristics in vertically aligned TiS_2 nanowall network grown using atomic layer deposition. *Mater. Res. Express* **6**, 115549 (2019).
34. Zhang, Z. *et al.* A self-forming composite electrolyte for solid-state sodium battery with ultralong cycle life. *Adv. Energy Mater.* **7**, 1–11 (2017).
35. Duchêne, L. *et al.* A stable 3 V all-solid-state sodium-ion battery based on a closo-borate electrolyte. *Energy Environ. Sci.* **10**, 2609–2615 (2017).
36. Yamauchi, H. *et al.* Pressureless all-solid-state sodium-ion battery consisting of sodium iron pyrophosphate glass-ceramic cathode and β″-alumina solid electrolyte composite. *J. Am. Ceram. Soc.* **102**, 6658–6667 (2019).
37. Hayashi, A., Noi, K., Tanibata, N., Nagao, M. & Tatsumisago, M. High sodium ion conductivity of glass-ceramic electrolytes with cubic Na_3PS_4. *J. Power Sources* https://doi.org/10.1016/j.jpowsour.2014.02.054 (2014).
38. Niu, W., Chen, L., Liu, Y. & Fan, L. Z. All-solid-state sodium batteries enabled by flexible composite electrolytes and plastic-crystal interphase. *Chem. Eng. J.* **384**, 123233 (2020).
39. Yao, Y. *et al.* Toward high energy density all solid-state sodium batteries with excellent flexibility. *Adv. Energy Mater.* **10**, 1–9 (2020).
40. Yu, X., Xue, L., Goodenough, J. B. & Manthiram, A. A high-performance all-solid-state sodium battery with a Poly(ethylene oxide)-$Na_3Zr_2Si_2PO_{12}$ composite electrolyte. *ACS Mater. Lett.* **1**, 132–138 (2019).
41. Zhao, C. *et al.* Revealing an interconnected interfacial layer in solid-state polymer sodium batteries. *Angewandte Chemie Int. Ed.* **58**, 17026–17032 (2019).
42. NIST X-ray photoelectron spectroscopy database.
43. Su, J. *et al.* The effect of Fe2 ions on dielectric and magnetic properties of $Yb_3Fe_5O_{12}$ ceramics. *J. Appl. Phys.* **111**, 3–7 (2012).
44. Atsunori, M., Hirotada, G. & Phuc, N. H. H. Preparation of cubic Na_3PS_4 by liquid-phase shaking in methyl acetate medium. *Heliyon* **5**, e02760 (2019).
45. Wu, E. A. *et al.* A stable cathode-solid electrolyte composite for high-voltage, long-cycle-life solid-state sodium-ion batteries. *Nat. Commun.* **12**, 1–11 (2021).
46. Tanibata, N., Hayashi, A. & Tatsumisago, M. Improvement of rate performance for all-solid-state $Na_{15}Sn_4$/amorphous TiS_3 cells using $94Na_3PS_4{\cdot}6Na_4SiS_4$ glass-ceramic electrolytes. *J. Electrochem. Soc.* **162**, A793–A795 (2015).

Acknowledgements

This work was partially supported by Grants-in-Aid for Scientific Research (Grant Nos. 19H05815, 19K15657, 20H02436, 21H01625, 21J14422, and 21K14715) from the Ministry of Education, Culture, Sports, Science, and Technology (MEXT), Japan; a CREST grant from the Japan Science and Technology Agency, Japan (Grant No. JPMJCR21O6); and the Data Creation and Utilization-Type Material Research and Development Project (grant number, JPMXP1122712807) from MEXT; Takahashi Industrial and Economic Research Foundation; The Naito Science & Engineering Foundation; Fujikura Foundation.

Author contributions

N.T. conceived and designed the experiments: N.N. and K.M. performed the experiments and analysed the data: H.T. contributed materials/analysis tools: N.T. and M.N. co-wrote the paper.

Competing interests

The authors declare no competing interests.

Additional information

Supplementary Information The online version contains supplementary material available at https://doi.org/10.1038/s41598-024-53154-5.

Correspondence and requests for materials should be addressed to N.T.